



**Kapteyn  
Institute**

**RuG**

Rijksuniversiteit Groningen  
*Department of Astronomy*

University of Groningen  
BACHELOR RESEARCH PROJECT

April 11, 2012

---

# Spectral analysis of the cooling phase of an x-ray superburst in 4U 1636-53

---

*Author:*  
Gerjon MENSINGA

*Supervisors:*  
Prof. Dr. Mariano MÉNDEZ  
Guobao ZHANG, MSc.

---

# CONTENTS

<b>1</b>	<b>Introduction</b>	<b>3</b>
<b>2</b>	<b>Data Information</b>	<b>5</b>
<b>3</b>	<b>Method</b>	<b>7</b>
3.1	The XSPEC software . . . . .	7
3.2	Data fitting in XSPEC . . . . .	9
3.3	Colors and types of X-ray bursts . . . . .	10
<b>4</b>	<b>Analysis</b>	<b>12</b>
4.1	Blackbody model . . . . .	13
4.2	Adding the power-law component . . . . .	14
4.3	Iron emission line and absorption edge . . . . .	15
4.4	F-test for comparing models . . . . .	16
4.5	The wabs*(bbodyrad + powerlaw + gaussian)*edge model . . . . .	18
<b>5</b>	<b>Color correction and metallicity</b>	<b>21</b>
<b>6</b>	<b>Discussion</b>	<b>23</b>
<b>7</b>	<b>Acknowledgements</b>	<b>24</b>

## Abstract

We analyzed the cooling phase of an x-ray superburst of the low-mass X-ray binary 4U 1636-53 using different models in XSPEC software. Our goal was to find the behavior of certain properties of the neutron star, e.g. radius and temperature, and to find the chemical composition of the neutron star atmosphere. We tried 6 different models for the cooling phase of the superburst and found that the best fit came from a model consisting of a blackbody, a power law, a gaussian emission line and an absorption edge. We found that the bolometric flux versus blackbody temperature relation,  $F \propto T_{bb}^4$ , does not hold, telling us that the blackbody radius changes over time. We also conclude from the color-correction factor that the superburst is a product of metal burning, fueled most likely by carbon.

---

---

# CHAPTER 1

---

## Introduction

For this research we have studied a so called X-ray superburst in the neutron-star x-ray binary (NSXRB) 4U 1636-53, also known as V801 Ara. X-ray superbursts are different from the more common 'standard' bursts on neutron star surfaces, mainly because the cooling time takes a few hours, instead of just seconds. (Strohmayer and Brown, 2002)

The physical processes of superbursts are still mainly unknown and therefore widely researched. In this thesis we try to find more information about why the superburst is happening, how the chemical composition of the stellar atmosphere varies during the cooling phase of the superburst, and how the surroundings of the star affects the detected photons of the burst.

A neutron star is star at the end of its life cycle. The three possible (observed) end stages of a star are white dwarfs, neutron stars and black holes (barring possible quark stars). A neutron star is formed when the mass of the progenitor star is roughly between  $1.4M_{\odot}$  and  $\sim 3M_{\odot}$ . The gravitational pressure of such stars is so high that it will force protons and electrons to combine and form neutrons. The star will become one ball of (mostly) neutrons in the interior with an electron-ion plasma near the surface.

An X-ray burst is due to a thermonuclear, unstable burning process on the neutron star surface. For X-ray bursts to occur we need to have matter accreted on the neutron star surface. This way pressure is build up on the surface until it reaches the nuclear burning threshold. Since the accreted matter has to come from somewhere, we need a so called 'feeder' that provides our star with matter. That is the reason why X-ray bursts happen in binary systems in which two objects orbit each other very closely. Because of the relatively small distance between the two stars in a binary system, they are greatly influenced by each others gravity. Gas on the upper layers of each star will deform into an ellipsoidal shape. As long as the gas stays within the Roche Lobe (RL), the Roche Lobe is the region in the system in which the gas is still gravitationally bound by its 'parent' star, there will be no exchange in gas. In our NSXRB the gravitational potential of the neutron star is much higher than that of the companion star, causing the RL of the companion star to overflow - thereby accreting matter onto the neutron star surface which, by the rapid (582 Hz for 4U 1636-53 (Zhang et al., 1997)) spin of the neutron star, forms an accretion disc around it. It is believed that due to the spiralling of the accretion disc as it falls upon the neutron star it will, by conservation of angular momentum, make the neutron star rotate faster an faster. Eventually the neutron star will cannibalize its companion completely. What is left is an isolated, rapid spinning neutron star. It is assumed that this process is a possible origin of millisecond pulsars (Radhakrishnan and Srinivasan, 1982).

Accreted matter (mostly hydrogen, some helium and metals) of the companion star in the accretion disc will fall to the neutron star surface where it is equally spread over the entire surface due to the spinning of the neutron star. If this accretion process happens for a longer period of time, the pressure on the neutron star surface will increase until the pressure becomes so high that it will ignite hydrogen and helium burning, creating heavier elements (e.g. carbon and oxygen). During this thermonuclear burning process there is a huge increase in intensity of the neutron star surface. This process can be seen as a peak in the intensity from the neutron star surface. It is called a burst because the increase in intensity due to the burning is very short (the intensity increase lasts only a few seconds).

Since the launch of X-ray satellites like RXTE and BeppoSAX, there has been a close look to the X-ray sky. Cornelisse et al. (2000) were the first to publish about a different type of X-ray burst in the low mass X-ray binary (LMXB) 4U 1735-44. This burst was, with 86 minutes, significantly longer than 'normal' X-ray bursts. Over the following years six more binary sources showed these long bursts, which were dubbed 'superbursts'.

A superburst is a special kind of burst that happens in LMXBs. While a normal burst takes only a few seconds, a superburst takes several hours before the neutron-star surface is cooled down to its pre-burst temperature. This decay time-scale is in agreement with the cooling time of a carbon layer of 10 - 100 meter thick (Strohmayer and Brown, 2002; Cumming and Macbeth, 2004). The cooling phase of the superburst in this thesis took roughly 7 hours before it reached its pre-burst intensities again.

At the moment of writing there are eleven different LMXBs known that have produced a (candidate) superburst (Keek and Heger, 2011). 4U 1636-53 has produced 2 observed superbursts until now, occurring 4.7 years apart.

It is still not certain why this kind of superbursts occur. One of the possibilities, as introduced by Strohmayer and Brown (2002), is that the bursts of the neutron star turns the hydrogen into helium and helium into metals, most likely carbon. This carbon will, because it is heavier than hydrogen and helium, sink deeper into the atmosphere of the neutron star, creating a 'layer' of carbon beneath a 'layer' of hydrogen/helium. With each burst the carbon abundance on the lower layers of the neutron star will increase. When the pressure in the carbon layer becomes high enough, it will ignite carbon burning. This kind of process takes longer to cool down than a normal burst and is therefore one of the possible explanations for superbursts.

Analysis of X-ray superbursts have been done before on 4U 1636-53, and other neutron star LMXBs. Examples are the analysis for a superburst in LMXB 1454-69 (in't Zand et al., 2003), in which a blackbody model and a bremsstrahlung correction was used to analyze the superburst, and the superburst of 4U 1820-30 (Strohmayer and Brown, 2002), where a combination of a blackbody model with an iron emission line and absorption edge proved the best fit.

In this thesis we analyze the time-resolved spectra of a superburst in 4U 1636-53. From the spectra we deduce the evolution of properties of different spectral components to try and find out what kind of processes happen during the burst.

---

---

# CHAPTER 2

---

## Data Information

The data that is used in this research comes from an observation of a superburst of the LMXB 4U 1636-53. It was captured by the Rossi X-ray Timer Explorer telescope (RXTE). The total observation gives us 40000 seconds, or roughly 11.5 hours, worth of data. The observation was made on Februari 22 and 23 2001.

The plot of the intensity of the source as a function of time is seen in Figure 2.1.

Figure 2.1 shows a few gaps in the data, which are produced by occultations of the source during the orbit of the satellite around the Earth.

The moment of the burst is quite obvious in the graph. This happens at around 11000 seconds from the start of the observation (which was at Februari 22, 2001 16:56 UTC) and shows an increased count rate of over 5 times its normal (persistent) value. To make it easier to analyse, we split the data in stretches of 16 seconds each, starting from the moment of the burst. This results in 501 intervals together spanning 14000 seconds.

The red part of Figure 2.1 shows the 501 16-second time intervals we used in our analysis. The data that we analyzed consists of 3 main parts that are separated by the observation gaps caused by the occultations. The blue part indicates data of the pre- and post-burst observations and are used to determine the level of persistent emission of the source (the emission before and after the burst, due to accretion onto the neutron star). We need to correct for the persistent emission in order to obtain the net emission of the burst. The green points in the graph show the ignition stage of the burst. These are not included in the calculation of the background nor were they analyzed since they are not part of the cooling phase of the superburst.

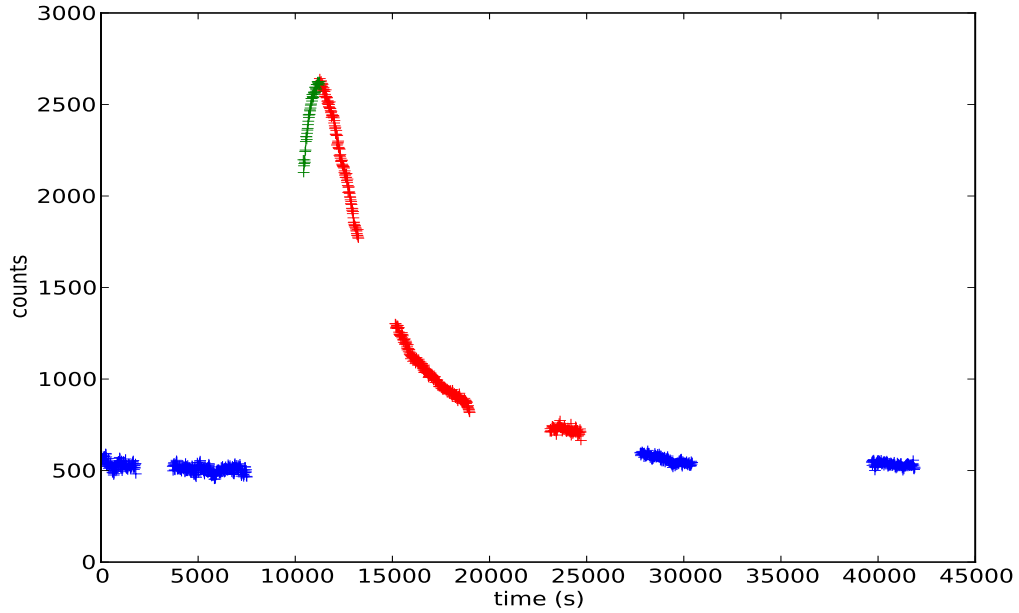


Figure 2.1: Intensity versus time plot of the 4U 1636-53 superburst. The superburst can be plainly seen starting at  $t \sim 11000$  seconds after the start of the observation on February 22, 2001 16:56 UTC. The red part of the graph shows the cooling phase of the superburst and is the data we analyze. The blue part gives the data points of the observation outside the superburst. There is a persistent emission coming from the source (as seen in the first 10000 and the last 20000 seconds); we have corrected for this persistent emission by subtracting it from the rest of the data. We can not be sure that this emission is constant during the burst, but since we are unable to find out exactly how it behaves, our assumption is that it remains constant during the superburst. The ignition of the superburst is in green and is not analysed since it is not a part of the cooling phase.

---

---

# CHAPTER 3

---

## Method

### 3.1 The XSPEC software

We analyzed the data using the XSPEC package (REF), which is used often for X-ray spectral analysis (Arnaud, 1996). We will describe shortly how we used XSPEC on our data.

To produce the data we use the software FTOOLS (version June 2011) and 'saextrct'. Saextrct is used to extract the spectrum and the lightcurve from the data. We use standard-2 (std2) data, which means we get our spectra in 16 seconds intervals and 129 channels covering the  $\sim 2$ -60 keV energy range.

To be able to analyse the spectra with XSPEC, we create a response file with the FTOOLS command 'pcarsp'. This creates a .rsp file for the std2 data. With FTOOLS we also created our background file, using the command 'pcabackest'. We describe the fitting procedure with XSPEC in the next section.

With this we have all the components we need and we can start playing with our data. In Figure 3.1 we see a plot of a randomly selected interval during the decay of the superburst made with XSPEC. The figure shows a logarithmic plot of source count rate per unit energy per unit area versus energy.

To find out what kind of processes contribute to our spectrum, we can make XSPEC fit different models to our data. XSPEC has quite a few build-in models to analyse spectral data. Basically what we do is plot our 16-second spectra in a [countrate, energy] plot and try to find a model that best fits these spectra. With the models we try to find out what processes are likely to take place in and around our source during the burst. In this research we have tried six different emission and absorption components to model our data. These are chosen because these components are most likely to play a role. The components we used (in different combinations) are listed below

#### **wabs**

This component accounts for interstellar absorption along the line of sight to the source. It has one parameter, which is the column density of hydrogen along the line of sight.

#### **bbbodyrad**

This component represents the spectrum of a blackbody emitter. It also takes into account the fact that our emitting blackbody can radially expand during the burst process. The parameters of the fit are the blackbody temperature ( $T_{bb}$ ) and the blackbody normalization ( $N_{bb}$ ) which represents the emitting area (A) of the blackbody.

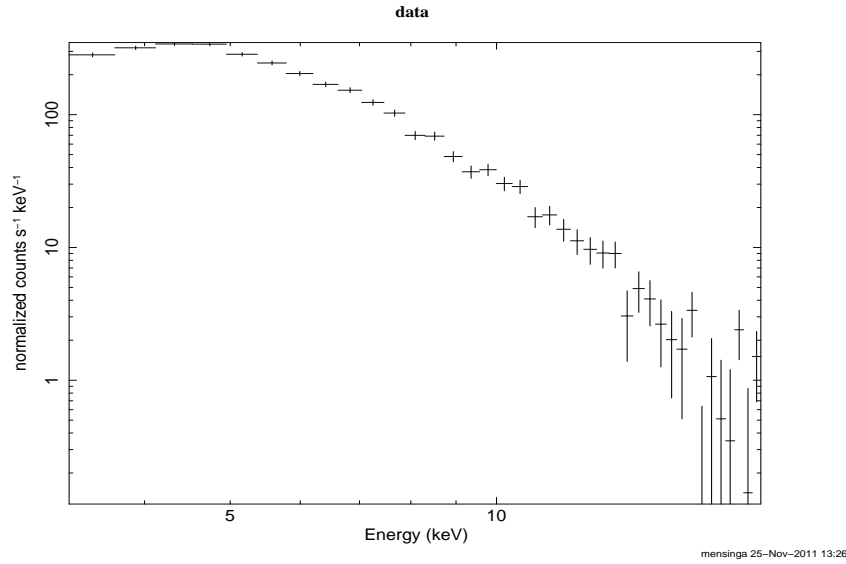


Figure 3.1: A typical plot of the energy spectrum from one of our (randomly chosen) data files created with the /xw plotting device in XSPEC. It is a logarithmic [counts, energy] plot. The energy range of 3.0-20 keV has been chosen because this is the range in which the instrument is properly calibrated.

### powerlaw

This model is a phenomenological description of the inverse Compton scattering (ICS) of the photons. With this model we include the fact that photons will scatter off relativistic electrons, thereby gaining energy, producing the high-energy part of the spectrum. The parameters of the model are the power-law index ( $\Gamma$ ) and normalization ( $N_{pl}$ ). The power-law can be caused by a corona around the star, or some other type of hot inter-stellar plasma. The fitted formula of the power-law spectrum is:  $F_{pl}(E) = N_{pl}E^{-\Gamma}$ .

### gaussian

A gaussian profile can be used to fit emission lines, taking into account emission by atoms and ions in the accretion disk. The element we included was the possibility of Iron-line emission, because iron is one of the most abundant heavy elements in the universe. Iron emission lines are seen between 6.4 keV for FeI, and 6.97 keV for FeXXVI. Fe emission lines are likely produced in the accretion disc around the star. The components of the gaussian model are the energy of the emission line ( $E_{gau}$ ), the width of the line ( $\sigma$ ), and the normalization ( $N_{gau}$ ).

### edge

Edge includes possible absorption by neutral or ionized material around the accretion disk. Again we assume only Iron absorption. The edge absorption is caused by the accretion disk around the star. Model components of Edge include the edge energy ( $E_{edge}$ ), and the optical depth ( $\tau_{max}$ ).

## 3.2 Data fitting in XSPEC

The way XSPEC fits the data is with a method that is known as forward fitting. The telescope has its own influence on the spectrum that we are working on - it can for example be more sensitive for certain energies, or it might have some more read-out noise in some part of the imaging device. All these instrumental influences together give the response function of the telescope. The formula you can assign to the forward fitting method is:

$$O(ch) = \int_0^{\infty} I(E) \cdot R(E, ch) dE \quad (3.1)$$

Here  $I(E)$  is the incoming spectrum and  $R(E, ch)$  is the response function of the telescope. The response of the telescope depends not only on energy, but also on the channel in which your energy is located.

We know the response of the telescope,  $R(E, ch)$ , and - after measurement - we know the outcome,  $O(ch)$ , which is a function of channel. Because both  $R(E, ch)$  and  $O(ch)$  have errors, it is not correct to just simply invert the equation and calculate  $I(E)$ , because the errors in  $O(ch)$  and  $R(E, ch)$  will propagate and reflect in large errors in  $I(E)$ .

To avoid this problem we *assume* we know the incoming spectrum - lets call it  $I'(E)$ . The goal of  $I'(E)$  is that if we implement  $I'(E)$  in the equation we get a value  $O'(ch)$  that is very close to  $O(ch)$ .

$$O'(ch) = \int_0^{\infty} I'(E) \cdot R(E, ch) dE \quad (3.2)$$

So the case in this thesis is that we have various  $O(ch)$ . Then we define a model to fit the data with, e.g. `wabs(bbodyrad)`, which is the  $I'(E)$ , and we fit it with the spectrum  $O(ch)$ . If the model fits the spectrum well, which means  $O(ch) \sim O'(ch)$ , the reduced  $\chi^2$ , a measurement of average deviation of the data from the model, will be around unity and apparently is close to the true spectrum. If the reduced  $\chi^2$  is significantly higher (or lower), our model does not resemble reality and thus is discarded.

An example of such a fitting result is given in Figure 3.2, where the `wabs(bbodyrad)` model is plotted for the same data as in Figure 3.1. The top picture shows the data with the model, the bottom picture shows the deviation of the model (straight line) from the data (crosses).

After the model is fitted to the data, we extract the parameters of the model that give the best fit, fit the model with all our data files, and plot the parameters as a function of time. By analysing how the parameters vary with time, we try to explain what happens during the burst. The fitting is done using  $\chi^2$ -statistics. The  $\chi^2$  is given by:

$$\chi^2 = \sum_i^N \left[ \frac{|D_i - M_i|}{\sigma_i^2} \right] \quad (3.3)$$

Here  $D_i$  is the data value in point  $i$ ,  $M_i$  is the model value in point  $i$ , and  $\sigma^2$  is the standard deviation of point  $i$ . From the  $\chi^2$  the reduced  $\chi^2$  can be calculated using:

$$\chi_{red}^2 = \frac{\chi^2}{N_{dof}} \quad (3.4)$$

Or the reduced  $\chi^2$  is the  $\chi^2$  of our data with respect to the model divided by the number of degrees of freedom the model gives us. The number of degrees of freedom is gained by subtracting the number of parameters of the model from the number of fitted data points. The closer the reduced  $\chi^2$  is to unity, the better the model fits our data.

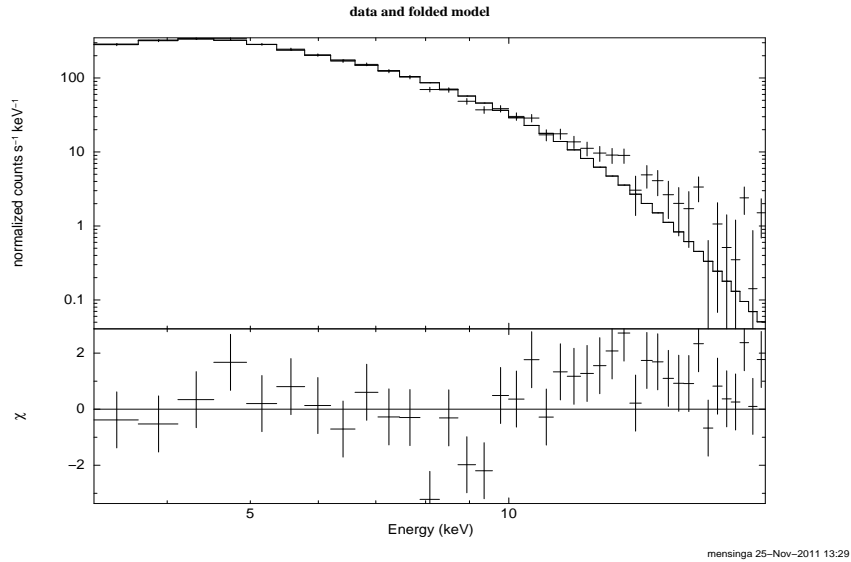


Figure 3.2: Same data set as in Figure 3.1, here fitted with the `wabs(bbodyrad)` model. Below is the deviation,  $\chi^2$ , of the model from the actual data. A perfect fit would mean that all the data points would be consistent with the line.

As a final note I want to comment about bad data files. Some files are for some reason not good data. This can be because a 16 second data file did not actually consist of 16 seconds, or because the measurement misses data above or below a certain energy value. These data are easily filtered out (mainly because they give extreme reduced  $\chi^2$  values). The corrupted data files have been closer examined and have been excluded for valid reasons like the ones stated above. The number of corrupted files omitted varied a little with our arbitrary boundaries, but were always below 10.

### 3.3 Colors and types of X-ray bursts

We can see in Figures 3.1 and 3.2 that the intensity in the higher energies can be up to a few orders of magnitude lower in comparison with the count rate of the lower energies. This implies that the superburst is happening in a 'soft state', which means the integrated intensity over the low energy band is higher than the integrated intensity over the high energy band.

To find if this is consistent with the spectral properties of the source right before the burst, we check if the persistent emission right before the burst is happening in a relative soft state as well. This can be done by finding out in which 'color' the persistent emission is radiating. You can find the color of an X-ray source by dividing the spectrum in four equidistant sections on the energy axis. The soft color is defined as the second quarter divided over the first, the hard color is defined as the fourth quarter divided by the third. The soft color and hard color can then be put into a color-color diagram.

In Figure 3.3 we can see the color-color diagram with a collection of persistent emissions of 4U 1636-53. The shape of this diagram is dubbed as an 'Atoll' (Hasinger and van der Klis, 1989). The Atoll shape consists of an 'island state', or hard state, which is located above the blue line, and a 'banana state', or soft state, which is below the blue line (Zhang et al., 2011). The blue line is chosen such that below it are all the Photospheric Radial Expansion bursts (PRE bursts), which means that the radius of the emitting blackbody expands during the burst before the cool-

ing phase. The non-PRE bursts lack this property. The non-PRE bursts are classified as 'hard non-PRE bursts' in the island state, and 'soft non-PRE bursts' in the banana state. The higher the soft color to high color ratio is, the bigger the luminosity of the source. It is assumed that the mass accretion rate is rising if you move from the island state, to the lower banana and then to the upper banana (Hasinger and van der Klis, 1989).

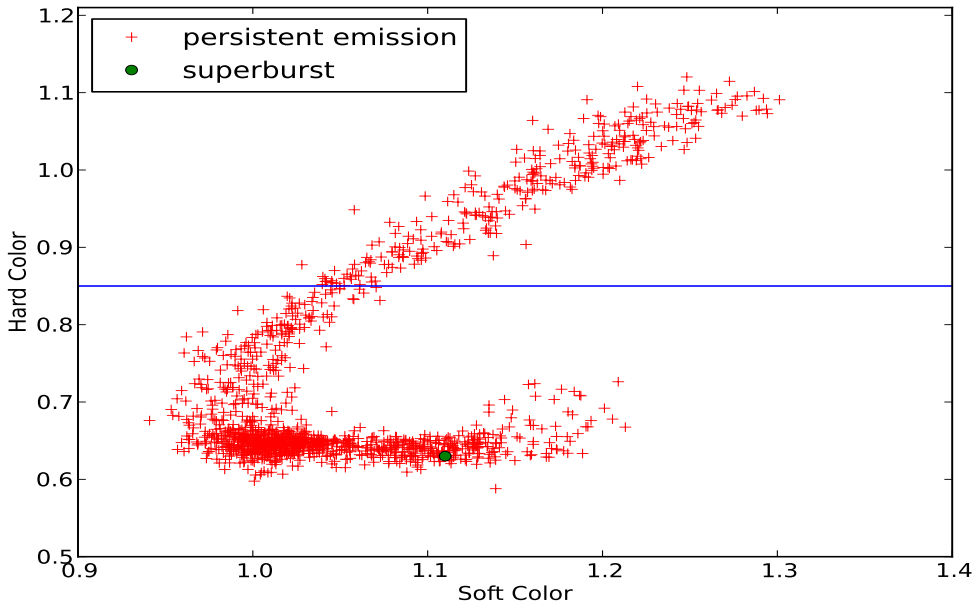


Figure 3.3: Color-color diagram of persistent emissions of 4U 1636-53. The persistent emission of the source at the time of the superburst is given by the green dot in the graph. It can be seen that the superburst occurs when the source is in the upper banana region, implying a relatively large mass accretion rate. The values are normalized with the hard and soft color values of the crab nebula. Thanks go to Guobao Zhang for providing us with the relevant data.

In Figure 3.3 the green dot locates the position of the persistent emission of the source just before the superburst, by which we can see that the persistent emission before the superburst happens in the upper banana state, which means there is a relatively high mass accretion rate when the burst occurs. This is in agreement with the superburst model by Keek and Heger (2011). They found that their model worked best on 4U 1636-53 if they gave it a mass accretion rate that was four times higher ( $0.40\dot{M}_{Edd}$ ) than average mass accretion rate of this source over the past few decades, which is  $0.12\dot{M}_{Edd}$ .

To analyse all data files in quick succession we wrote python scripts within XSPEC to fit the model automatically to all data. XSPEC in python (pyXSPEC) is a program that is still under development. Nevertheless, pyXSPEC is relatively easy to use, and was very helpful for this project. Therefore many thanks go to its programmer, Weiwei Zhu.

---

---

# CHAPTER 4

---

## Analysis

Now that we know how and what we do, it is time to describe some results. We analysed the data only in the energy range between 3.0 and 20 keV, because this is the spectral region in which RXTE is well calibrated. In this energy region there are 39 data points, which is important to know for determining  $N_{dof}$  and for the calculation of the reduced  $\chi^2$ .

Since our goal is to understand the net emission of the burst, which is superimposed to the persistent emission of the source due to continued accretion onto the neutron star, we subtracted the contribution of the persistent emission from the individual spectra for our analysis. We fitted each model to the data using two different persistent spectra as backgrounds. Background 1 (B1) is the average measurement of the source spectrum before the burst, the average of roughly the first 8000 seconds in Figure 2.1. The second background (B2) is the average of the source spectrum after the burst, so the average after 35000 seconds in Figure 2.1. The reason to test our fits using these two separate backgrounds is that accretion likely continues during the superburst, and hence B1 and B2 may not provide the actual background during the superburst. Using these two separate intervals provides an estimate of the systematic uncertainties of our results due to our lack of knowledge of the true persistent emission background during the superburst.

During the analysis it became clear that the difference in effects of the two different backgrounds were insignificant. Both the B1 and B2 analysis has been done, but the results from the B2 analysis is so similar to the analysis of B1, that it is not deemed fruitful to analyze the outcomes of the two backgrounds as two different results. The results we describe below all use B1.

Another variable that is useful to look at is the [Bolometric Flux, Temperature] relation. Since the bolometric flux of a blackbody goes as  $F_{bol} \propto T_{eff}^4$ , assuming that the emitting area (radius) is constant, we should find a straight line on a log-log plot in a [Flux, kT] graph. If it is not a straight line, it can be because the emitting area is not constant, or that the fitted (blackbody) temperature is not equal to the effective temperature of the neutron star.

## 4.1 Blackbody model

To start off easy, we kept our model relatively simple at first by using the model `wabs*(bbodyrad)`. The component `wabs` is used in all the models that we try, for the interstellar absorption is always present, and does not vary or disappear over time. The interstellar absorption depends on the column density of hydrogen atoms,  $n(\text{H})$ , in the interstellar medium along the line of sight, for a given assumed energy-dependent cross section and abundance of the interstellar medium. Pandel et al. (2008) determined that the hydrogen column density towards 4U 1636-53 is:  $n(\text{H}) = 0.36 \times 10^{22} \text{ cm}^{-2}$ . Because this parameter is fixed it will not influence the  $N_{\text{dof}}$  of the models. The `bbodyrad` component is also used in each model. The blackbody emitter is present in any thermonuclear burning process, so because of this physical reality we are bound to use the blackbody as the basis of every model that we use. The parameters of the blackbody model are the blackbody temperature ( $T_{\text{bb}}$ ) and the blackbody normalization ( $N_{\text{bb}}$ ). From the normalization we compute the radius ( $R$ ) of the emitting area of the neutron star by using the relation:

$$R = \sqrt{\left[ N_{\text{bb}} \left( \frac{\text{distance}(\text{kpc})}{10\text{kpc}} \right) \right]^2} \quad (4.1)$$

$R$  has the units [km]. For the distance to our source we use 6 kpc (Galloway et al., 2008).

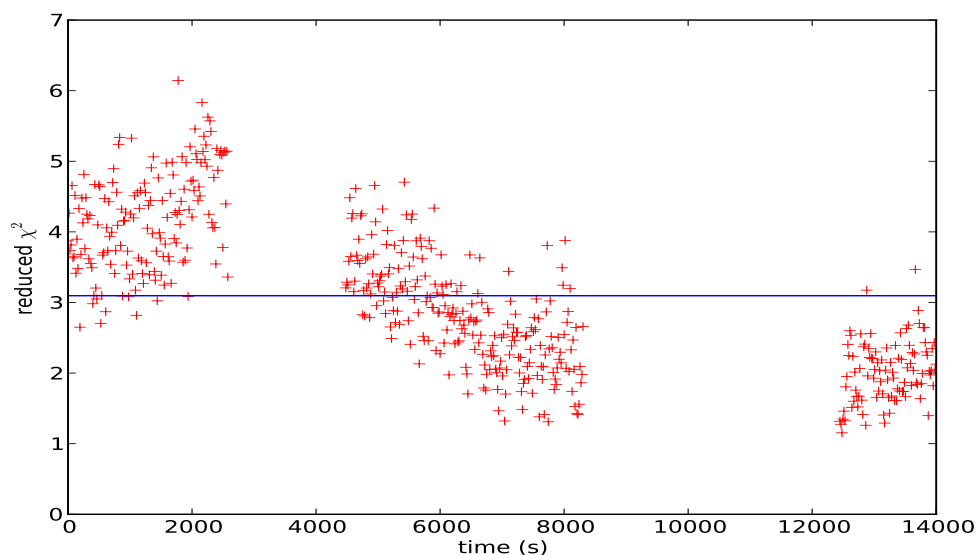


Figure 4.1: Reduced  $\chi^2$  of our Blackbody only model with 36 degrees of freedom. The average of the reduced  $\chi^2$  (the horizontal line) is over three, but for the first 5000 seconds it is even higher. The last third of the graph looks better which is due to the fact that the data can hardly be distinguished from the persistent background since the cooling phase is almost over (the background is well fitted with a blackbody in the hard color region).

This model quickly proved to be insufficient to describe the cooling phase. The reduced  $\chi^2$  is larger than one for all data points, with an average that is above 3 with 36 degrees of freedom. A blackbody model is not enough to describe the cooling phase of the superburst. Therefore we need a more complex model to describe our data correctly.

As we can see from Figure 4.1, the blackbody only model gives a much better result in the last third of the graph. This is probably the case because at that point the cooling phase is virtually over, so the persistent emission will overshadow some possible additional emission from the burst. Our background data fits better with the blackbody model than our data of the burst itself, thence the decrease in our reduced  $\chi^2$ . With this taken into account the average reduced  $\chi^2$  will be even higher if we assume the last part is irrelevant in this case.

## 4.2 Adding the power-law component

With only a blackbody model being insufficient, we next tried a more complex model by adding a power-law component: `wabs*(bbodyrad + powerlaw)`.

The power-law emission is due to the Inverse Compton Scattering (ICS) of soft photons coming from the neutron star in a hot electron plasma. When a soft (low-energy) photon comes into a hot plasma, it can gain energy by colliding with relativistic electrons, which have a higher energy than that of the photons. The electron will thereby transfer some of its energy to the photon, making the spectrum of the source harder. This can happen a number of times until the photon escapes the system, or the photon energy becomes as high as the electron energy so that the electrons become optically thin, causing the photons to not interact with the electrons anymore. The hot gas that produces the ICS is probably part of the accretion disk and/or a corona around the neutron star (Nikolaos, 2007).

The powerlaw has two parameters, called the photon index ( $\Gamma$ ) and the power-law normalization ( $N_{pl}$ ). The data show that  $\Gamma$  is between 1.5 and 3 for this source. The  $N_{pl}$  just gives the strength of the powerlaw in our data.

With an average reduced  $\chi^2$  of 1.68 for 34 degrees of freedom, this model already fits the data much better than the blackbody only model, although it is still formally unacceptable.

### 4.3 Iron emission line and absorption edge

For our next addition we expand the model with an iron emission line, and an iron absorption edge produced in the accretion disk. We constrained the energy of the line to be in the range of 6.4 - 7 keV (for FeI to FeXXVI), and the energy of the edge to 6.7 - 7.5 keV, because the FeI edge is around  $\sim 7.1$  keV. Using the gaussian and edge together is a bit risky, for it is possible that the emission line, which is a peak, overlaps with the edge, which is a gap. Therefore the gaussian and edge components can cancel each other out when they happen to overlap.

The parameters that are hereby added to our model are, for the emission line (that we represent by a gaussian profile), the emission energy of the line ( $E_{gau}$ ), the width of the line ( $\sigma$ ) and the normalization ( $N_{gau}$ ). The edge parameters are the edge energy ( $E_{edge}$ ) and optical depth ( $\tau_{max}$ ). After computing a model without a power-law and with a gaussian and/or an edge, we find an average reduced  $\chi^2$  that is varying between 2 and 2.2 (for 31 degrees of freedom). Hereafter we decided to use a power-law in all models we try, for that brings our average reduced  $\chi^2$  down to 1.7 or lower (see Section 4.2).

Thus the next model we will discuss is `wabs*(bbodyrad + powerlaw + gaussian)*edge`. This model gives an average reduced  $\chi^2$  of 1.28 for 29 degrees of freedom. The  $N_{gau}$  in this model however is very low ( $\sim 0.02$ ) and has some huge errors. To reduce the errors we rebinned the data, thereby losing information but gaining better defined values. The data has been rebinned so that 15 data points were combined to one point, as can be seen in Figure 4.2. These low normalization values imply that a gaussian line may not be that emphatically present in our system.

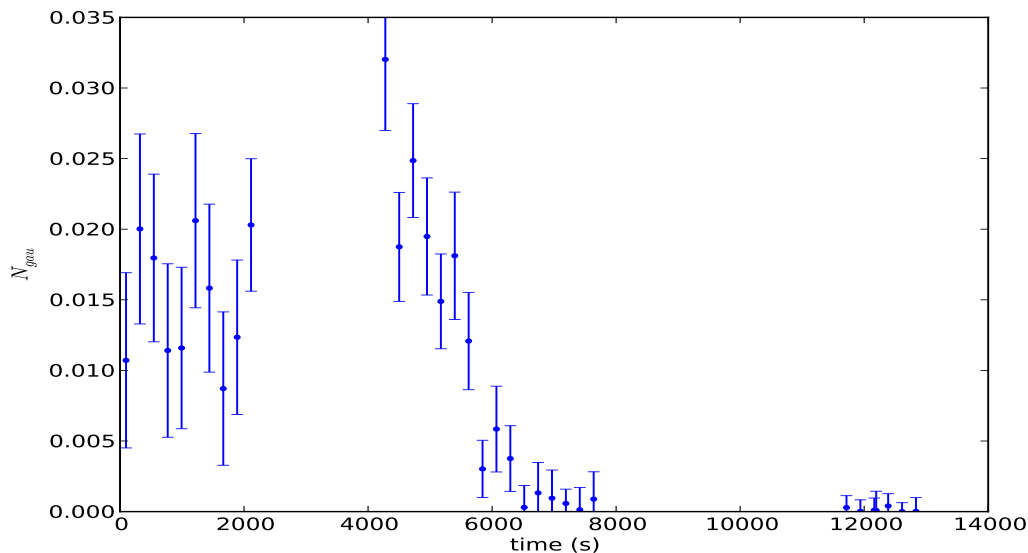


Figure 4.2: Normalization of the gaussian component. The low values imply a low relevance for an iron emission line. The data has been rebinned to reduce the errors in the data points (each point indicating a rebinning of 15 data points).

Our reduced  $\chi^2$  becomes a little higher if we omit the gaussian from our model altogether. The `wabs*(bbodyrad + powerlaw)*edge` model gives us an average reduced  $\chi^2$  of 1.31 for 32 degrees of freedom which is higher than the `wabs*(bbodyrad + powerlaw + gaussian)*edge` model. But since we only win 0.03 in our reduced  $\chi^2$  value the added gaussian component with the loss of 3 degrees of freedom one can ask if this loss in degrees of freedom is worth the gain in reduced  $\chi^2$ .

## 4.4 F-test for comparing models

Using the F-test command in XSPEC gave us the possibility to compare two different  $\chi^2$  distributions. The F-test is a statistical formalism which compares the  $\chi^2$  of one model with N degrees of freedom, with that of another model with M degrees of freedom ( $M \neq N$ ). The F-test compares the models and, with the values of the  $\chi^2$ , determines if the loss of degrees of freedom in the better defined model is statistically worth adding to our model or not. An F-value close to unity signifies a large likelihood that the added component does not add something statistically important to our model. An F-value  $\ll 1$  will mean that the more defined model is indeed adding something.

We did the F-test of the `wabs*(bbodyrad + powerlaw + gaussian)*edge` model versus the `wabs*(bbodyrad + powerlaw)*edge` model. The time evolution of the F-test gives us an average F-value that is around 0.1 for the first 5500 seconds. After that we see a rapid increase of the F-value to 1 after 5500 seconds. This is compatible with Figure 4.2, where the normalization of the gaussian is decreasing rapidly. This, however, does not mean the Iron line disappears. It is more likely we can't see the line anymore for statistical reasons. It might be that the count value becomes lower (which is plausible since the cooling phase has a lower temperature over time), or because the energy resolution of the satellite is not good enough to see the line.

We calculated the errors in XSPEC with a confidence level of  $2.7\sigma$ , or 90% confidence. The upper limit of the values are given by the value itself plus the higher errorbar. By defining the upper limit in this way we can say that there is a 95% chance for us to miss the iron line, if the value is below the upper limit. And since the upper limit is decreasing over time it is plausible that there is an iron line in the system that we fail to detect.

From this we conclude that although the `wabs*(bbodyrad + powerlaw)*edge` model gives the better fit (higher F-values) in the higher time intervals, we will assume that the `wabs*(bbodyrad + powerlaw + gaussian)*edge` model describes our system best since the Iron line is present in the lower time intervals and it can't just disappear.

For good measure we also calculated the F-test of `wabs*(bbodyrad + powerlaw)*edge` with `wabs*(bbodyrad + powerlaw)`. This gave very low probabilities (average of 0.007). From this we can say the edge component does add something influential to our model in comparison with the model with just a powerlaw component.

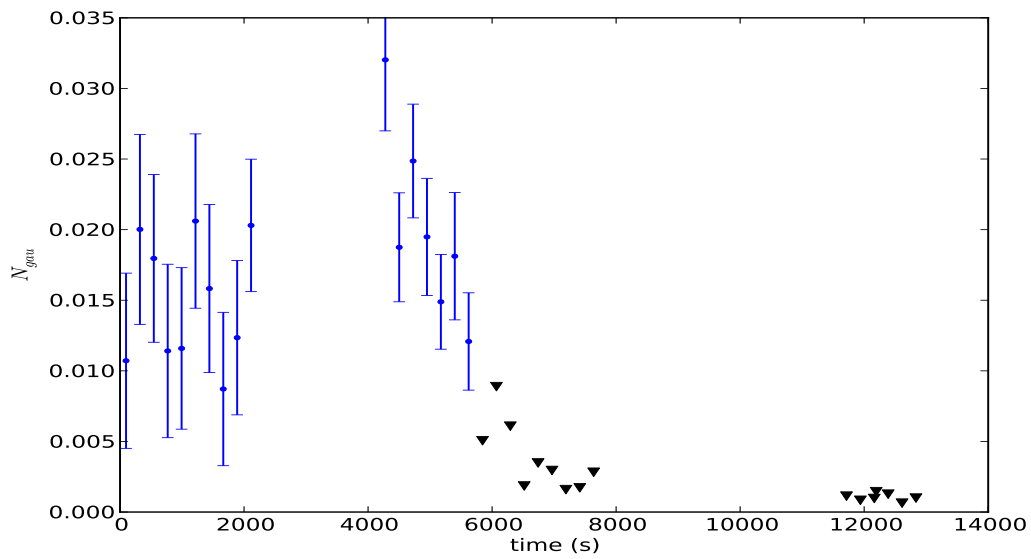


Figure 4.3: Normalization of the gaussian component. The low values imply a low relevance for an iron emission line. The data has been rebinned to reduce the errors in the data points (each point indicating a rebinning of 15 data points). The black triangles are giving the upper limit of the values. This implies that normalization values below  $\sim 0.005$  have a 95% change of being unnoticed by us.

## 4.5 The $wabs*(bbodyrad + powerlaw + gaussian)*edge$ model

In this section we will try to explain some of our results with graphs of our model components. We will concentrate on the model  $wabs*(bbodyrad + powerlaw + gaussian)*edge$ . We can see in Figure 4.4 that the reduced  $\chi^2$  of this model remains quite constant over the complete interval, which adds to the reliability of the model.

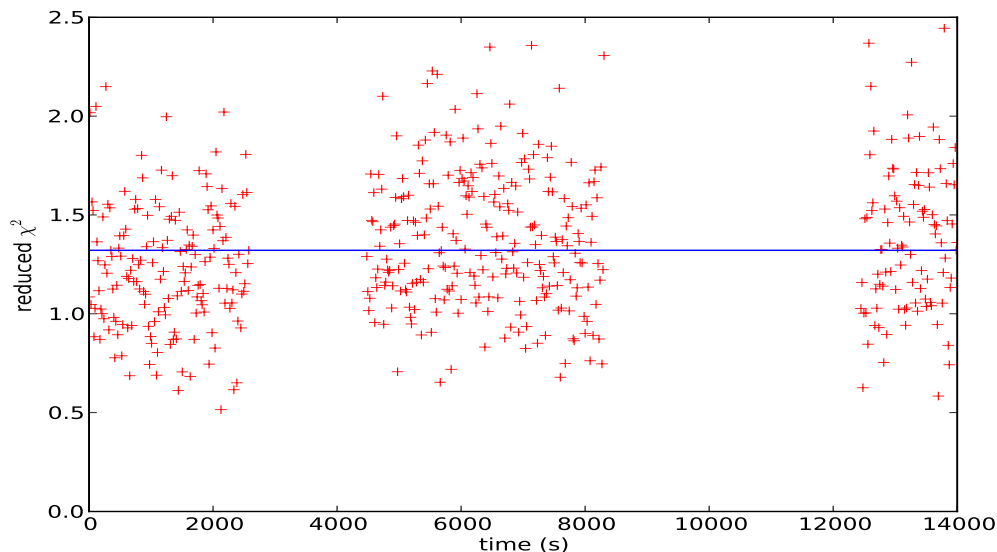


Figure 4.4: Reduced  $\chi^2$  of our best fitted model. It has an average of 1.32 (29 degrees of freedom) and remains quite constant over the complete time interval.

The main results of this model can be seen in Figure 4.5. We found that the temperature of our source over time follows the shape as in Figure 2.1 (also top graph of Figure 4.5). So it is seen as a peak in the beginning of the burst and an exponential decay after that. The temperature ranges from roughly 1.2 keV at the end to 2.3 keV at the peak which, after dividing by Boltzmann's constant, correspond to  $\sim 1.4 \times 10^7$  K and  $\sim 2.7 \times 10^7$  K respectively.

The radius is calculated from the blackbody normalization using Formula (4.1). The initial radius is 6 km, rises during the cooling phase to 8 km, and in the end decreases to around 5 km (where the distance is set at 6 kpc (Galloway et al., 2008; Zhang et al., 2011)). The uncertainty in our radius increases over time. Again we stress that the data in the end is less reliable since the cooling phase was as good as over at that time and is overshadowed by the persistent background emission.

The fact that our radius does not seem to be a constant quantity, means that our flux will not follow the  $T^4$  relation. In Figure 4.6 we enlarged the bottom graph of Figure 4.5. As we can see, the relation  $F_{bol} \propto T_{eff}^4$  does not hold. This implies that the emitting blackbody radius changes over time. However, following the example of Galloway et al. (2008) in the next section, the change in emitting area can also be due to a change in chemical composition in the neutron star atmosphere.

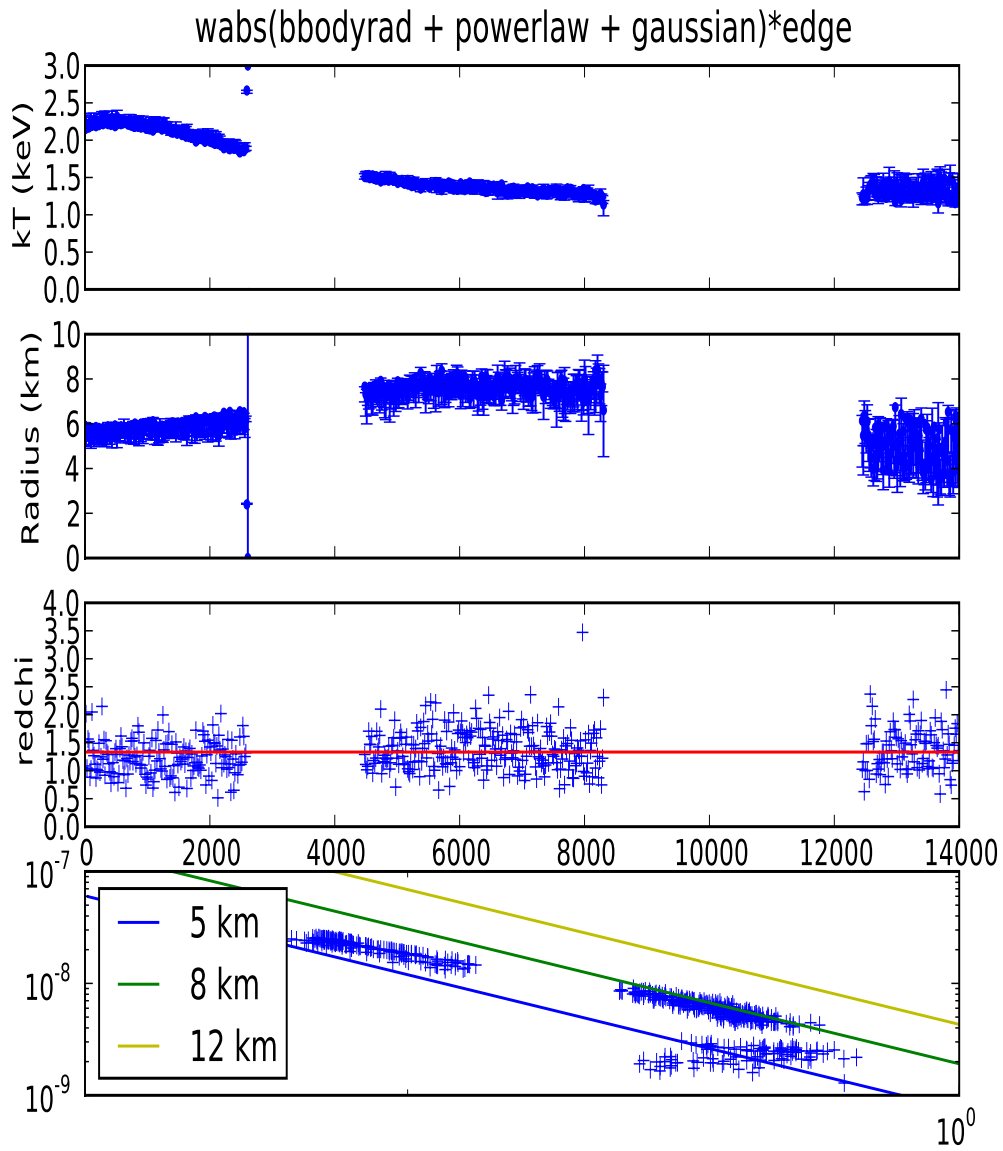


Figure 4.5: Plot of the `wabs*(bbodyrad + powerlaw + gaussian)*edge` model. The top graphs shows energy versus time, the one below that shows the radius of our emitting blackbody over time, the third shows the reduced  $\chi^2$  versus time (the horizontal line in the average value of the reduced  $\chi^2$ ), and the bottom shows the log-log plot of flux versus temperature. The 'horizontal' part of the bottom plot are the results for the last third of the measurement. These points do not follow the relation at all because they are background dominated. These points are omitted in Figure 4.6, which zooms in on the bottom graph.

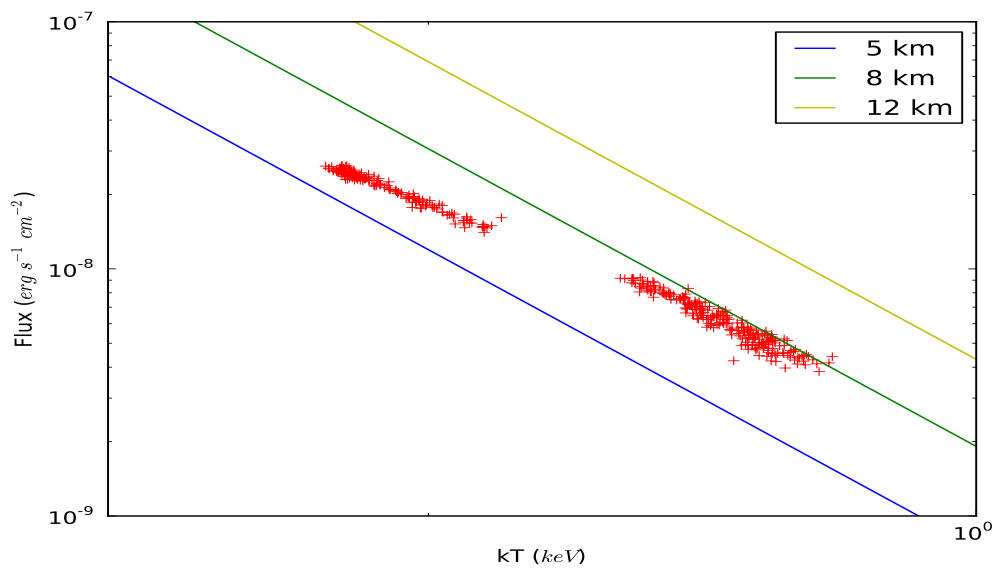


Figure 4.6: A log-log plot of the bolometric flux versus temperature of our best fit model. The three colored lines show the relation expected for a fixed (5, 8, or 12 km) emitting radius. Our data do not follow a straight line. It varies between 6 and 8 km, implying that the emitting blackbody radius of the source does not remain constant during the cooling phase.

---

---

# CHAPTER 5

---

## Color correction and metallicity

Now that we have found the best fitting model of the superburst in 4U 1636-53, we will try to find out what processes occur during the superburst. A good way to start is to try and determine the metallicity of the neutron star atmosphere during the superburst.

We will use the analysis method as described in Suleimanov et al. (2010) by which we calculate the color correction factor ( $f_C$ ). The color correction factor gives a correction of our blackbody spectrum. We get the temperature of our neutron star via the temperature component in the blackbody model. While the blackbody has a clearly defined shape (the Planck-curve), it gets distorted on its way to the telescope by scattering effects. So the emitted blackbody is different from the blackbody we observe. The color correction factor corrects for this distortion by re-creating the blackbody model for us the way it is presumably emitted from the neutron star surface. If we plot an  $[f_C, L/L_{Edd}]$  diagram we get a local minimum roughly between 0.1 and 0.3 of the luminosity. It turns out that higher metallicities ( $Z \sim Z_\odot$ ) tend to have a deeper minimum whilst small metallicities ( $Z \sim 0.01Z_\odot$ ) tend to have no clearly defined minimum.

The color correction factor can be calculated using:

$$f_C = \sqrt{\frac{R_\infty}{d\sqrt{\frac{F}{\sigma T_{bb}^4}}}} = \sqrt{\frac{R(1+z)}{d\sqrt{\frac{F}{\sigma T_{bb}^4}}}} \quad (5.1)$$

where  $R$  is the neutron star radius,  $d$  is the distance to the source,  $\sigma$  is the Stefan-Boltzmann constant and  $z$  is the gravitational redshift (Zhang et al., 2011). From our model we assume  $R = 9$  km,  $d = 6$  kpc and  $z = 0.36$ . We plot the results of our superburst with the table-model for the color correction factor for hydrogen burning, helium burning, and a superburst with a metallicity of one times solar taken from Suleimanov et al. (2010). The results are plotted in Figure 5.1.

The Eddington flux used in the graph for our superburst is not known. Since the Eddington flux is the flux in which the radiative pressure balances the gravitational pull, we have assumed that the Eddington flux is equal to the maximum luminosity of 4U 1636-53 in a PRE-burst (which is the luminosity at which the blackbody radius is maximum) which is around  $64 \pm 5 \times 10^{-9} \text{ erg cm}^{-2} \text{ s}^{-1}$  (Galloway et al., 2008). The plot shows that our superburst spectrum consists of, at least for a part, metal burning. This works in favour of the model of Strohmayer and Brown (2002).

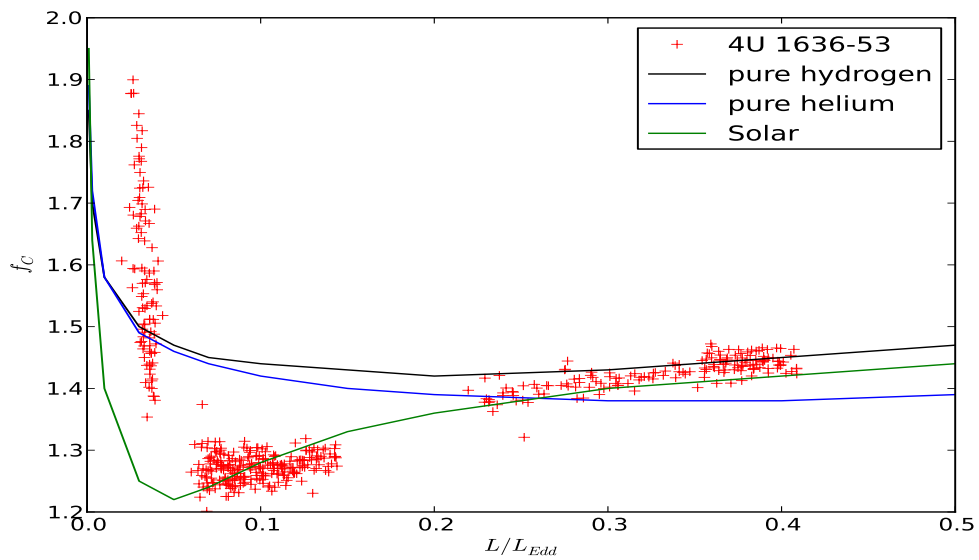


Figure 5.1: Color correction factor as a function of luminosity in Eddington units. Our burst has a clearly defined minimum, which is beneath the table values for pure hydrogen and helium burning. This indicates a certain amount of metal abundance in our chemical composition during the cooling phase.

---

---

# CHAPTER 6

---

## Discussion

In our research we found that the most likely environment of our neutron star during the superburst is described with the model `wabs*(bbodyrad + powerlaw + gaussian)*edge`. We conclude that the emitted photons are most likely exposed to a hot thermal plasma, a corona, around the star. Also there is some absorption of photons at higher energies because of the accretion disk, which also is causing an Iron emission line in our spectra. The values of the Iron line are mostly around 7 keV in the cooling phase, which means the Iron emission is dominated by the inner regions of the accretion disc (since there the disc is hotter, thus more ionized). Only in the second partial the line emission seems to come mostly from less ionized Iron. From the color correction factor it appears that the neutron star is burning a lot of metals during the superburst, from which we can say that a superburst is a product of at least a part metal, and probably mainly carbon, burning.

Analysis on the accretion disk around a superburst in 4U 1820-30 was done by Ballantyne and Strohmayer (2004). They used a spectral emission model to look at the evolution of the accretion disk around the neutron star during a superburst. They found that the inner radius of the accretion disk increases by roughly a factor 10 in the earlier stages of the burst. This can be due to the increase in the radiation pressure from the neutron star, pushing the inner disk away, or by heating of the gas by a radiation field, making it unable to produce emission lines.

Zhang et al. (2011) studied 288 X-ray bursts measured with RXTE from 4U 1636-53 up to May 2010. They found that almost none of the bursts (PRE and non-PRE) followed the bolometric flux-temperature relation,  $F \propto T_{bb}^4$ . This implies that either the emitting area or the color correction factor changes. By calculating the color correction factor they speculate that there is an enhanced abundance of metals in the neutron star atmosphere that is created during the burst.

Our results also show deviations from the bolometric flux-temperature relation. Since our color correction factor changes over time, we assume that this is because of a change of abundance in the neutron star atmosphere rather than a change in emitting radius. Because of the latter we are inclined to name this superburst a soft non-PRE burst (Zhang et al., 2011).

---

---

# CHAPTER 7

---

## Acknowledgements

I really enjoyed to do the research I have described above. It gave me the possibility to get my first taste in astronomical research and it gave me the experience of how it is to work with (and a little bit as) a full-time astronomer. I would like to thank **Mariano** and **Guobao** for their enthusiastic attitude, the fact that they were always ready to help me on my way and for making the research as enjoyable for me to work on as was possible. I'd also like to thank the other members of the **High Energy Astrophysics** group for their interesting meetings and their willingness to share their knowledge with me.

Of the less prominent heroes I'd like to thank **Casper** for making a reliable (and sometimes motivational) studie partner over the last few years and because he was always prepared to check if my python program was still working when it was running for over 15 hours and I was already gone celebrating weekend or something.

Last but not least I want to thank my parents **Henk** and **Caroline** for their support in my, already quite long, career as a student. The road was not as flawless as one would have hoped, but with their help and motivation I was able to avoid all obstacles that I found on my way.

---

# BIBLIOGRAPHY

- K. A. Arnaud. XSPEC: The First Ten Years. In G. H. Jacoby & J. Barnes, editor, *Astronomical Data Analysis Software and Systems V*, volume 101 of *Astronomical Society of the Pacific Conference Series*, page 17, 1996.
- D. R. Ballantyne and T. E. Strohmayer. The evolution of the accretion disk around 4U 1820-30 during a superburst. *ApJ*, 602:L105–L108, 2004.
- J. Cornelisse, R. Heise, E. Kuulkers, F. Verbunt, and J. M. M. in 't Zand. The longest thermonuclear X-ray burst ever observed? *ApJ*, 357(L21), 2000.
- A. Cumming and J. Macbeth. The Thermal Evolution following a Superburst on an Accreting Neutron Star. *ApJ*, 603:L37–L40, 2004.
- D. K. Galloway, M. P. Muno, J. M. Hartman, P. Savov, D. Psaltis, and D. Chakrabarty. Thermonuclear bursts observed by RXTE. *ApJS*, 179(360), 2008.
- G. Hasinger and M. van der Klis. Two patterns of correlated X-ray timing and spectral behaviour in low-mass X-ray binaries. *A&A*, 225:79–96, 1989.
- J. J. M. in't Zand, E. Kuulkers, F. Verbunt, J. Heise, and R. Cornelisse. A superburst from 4U 1254-69. *A&A*, 411:L487–L491, 2003.
- L. Keek and A. Heger. Multi-zone models of superbursts from accreting neutron stars. *ApJ*, 743:189, 2011.
- F. Nikolaos. Probing black holes spins with X-ray spectroscopy. Master's thesis, University of Utrecht, 2007.
- D. Pandel, P. Kaaret, and S. Corbel. The cooling phase of Type-I X-ray bursts in 4U 1636-53. *ApJ*, 688(1288), 2008.
- V. Radhakrishnan and G. Srinivasan. On the origin of the recently discovered ultra-rapid pulsar. *Current Science*, 51:1096–1099, 1982.
- T. E. Strohmayer and E. F. Brown. A Remarkable 3 Hour Thermonuclear Burst from 4U 1820-30. *ApJ*, 566:1045–1059, 2002.
- V. Suleimanov, J. Poutanen, and K. Werner. X-ray bursting neutron star atmosphere models: spectra and color corrections. *A&A*, 527:A139, 2010.
- G. Zhang, M. Méndez, and D. Altamirano. The cooling phase of Type-I X-ray bursts in 4U 1636-53. *MNRAS*, 413:1913–1921, 2011.

W. Zhang, I. Lapidus, J. H. Swank, N. E. White, and L. Titarchuk. U 1636-53. IAU Circ., 6541: 1, 1997.